BIOCHEMISTRY
including biophysical chemistry & molecular biology

Article

pubs.acs.org/biochemistry

HypD Is the Scaffold Protein for Fe-$(CN)_2CO$ Cofactor Assembly in [NiFe]-Hydrogenase Maturation

Sven T. Stripp,*[,†] Basem Soboh,[‡] Ute Lindenstrauss,[‡] Mario Braussemann,[‡] Martin Herzberg,[‡] Dietrich H. Nies,[‡] R. Gary Sawers,[‡] and Joachim Heberle[†]

[†]Experimental Molecular Biophysics, Freie Universität Berlin, Arnimalle 14, 14195 Berlin, Germany

[‡]Institute of Microbiology, Martin-Luther University Halle−Wittenberg, Kurt−Mothes−Straße 3, 06120 Halle (Saale), Germany

Supporting Information

ABSTRACT: [NiFe]-hydrogenases bind a NiFe−$(CN)_2CO$ cofactor in their catalytic large subunit. The iron−sulfur protein HypD and the small accessory protein HypC play a central role in the generation of the CO and CN^- ligands. Infrared spectroscopy identified signatures on an anaerobically isolated HypCD complex that are reminiscent of those in the hydrogenase active site, suggesting that this complex is the assembly site of the Fe-$(CN)_2CO$ moiety of the cofactor prior to its transfer to the hydrogenase large subunit. Here, we report that HypD isolated in the absence of HypC shows infrared bands at 1956 cm^{-1}, 2072 cm^{-1}, and 2092 cm^{-1} that can be assigned to CO, CN^1, and CN^2, respectively, and which are indistinguishable from those observed for the HypCD complex. HypC could not be isolated with CO or CN^- ligand contribution. Treatment of HypD with EDTA led to the concomitant loss of Fe and the CO and CN^- signatures, while oxidation by H_2O_2 resulted in a positive shift of the CO and CN^- bands by 35 cm^{-1} and 20 cm^{-1}, respectively, indicative of the ferrous iron as an immediate ligation site for the diatomic ligands. Analysis of HypD amino acid variants identified cysteines 41, 69, and 72 to be essential for maturation of the cofactor. We propose a refined model for the ligation of Fe-$(CN)_2CO$ to HypD and the role of HypC in [NiFe]-hydrogenase maturation.

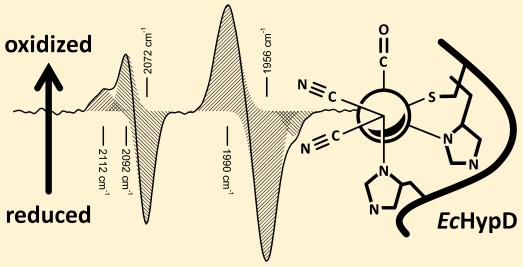

Hydrogenases catalyze the uptake and evolution of molecular hydrogen in a broad range of archaea, bacteria, and certain lower eukarya.[1] Different classes of hydrogenases can be distinguished depending on the composition of the cofactor in the catalytic subunit of the enzyme. [NiFe]-hydrogenases are typically heterodimeric, with a large catalytic subunit and a small ferredoxin-like subunit.[2] The large subunit coordinates a unique NiFe-$(CN)_2CO$ cofactor whose electron density has been detected by X-ray crystallography.[3] The chemical nature of the cofactor was elucidated by FT-IR spectroscopy[4] due to the specific absorption of the carbon monoxide[5,6] and cyanide ligands[7,8] in the mid-IR range. Hydrogenases are fast and extremely efficient catalysts. Because of the possibility of utilizing hydrogen as an alternative means of storing energy, it is important to understand the molecular principles of hydrogen activation. In order to do this, it is also essential to understand how the NiFe-$(CN)_2CO$ cofactor is synthesized *in vivo*.

The synthesis and introduction of the NiFe-$(CN)_2CO$ cofactor into the apo-catalytic hydrogenase large subunit requires a maturation apparatus comprising six key accessory proteins, termed HypA, B, C, D, E, and HypF.[9] Two of these accessory proteins, HypA and B, catalyze the acquisition and insertion of Ni into the hydrogenase apo-protein.[10] In a concerted reaction, HypE and HypF generate the CN^- ligands from carbamoylphosphate with the concomitant consumption of six equivalents of ATP. HypF transfers carbamate to the C-terminal cysteine of HypE to deliver thiocarboxamide.[11,12] ATP-dependent dehydration catalyzed by HypE yields a thiocyanate.[11,13] HypE forms a complex with HypC and HypD and presumably transfers the CN^- ligands to a Fe ion on HypD.[14]

HypD is a soluble iron−sulfur protein of 42 kDa, and the crystal structure of the ortholog from *Thermococcus kodakaraensis* has been determined to 2 Å.[15] Its tertiary structure consists of a unique C-terminal [4Fe−4S] cluster-binding motif plus two α/β domains termed I and II (the latter N-terminal). These α/β domains share identity with nucleotide-binding proteins and are categorized as Rossmann-folds.[16] Two conserved amino acid sequences line the active site, CGxH and PxHVS of domain II, and provide a rigid back to the hydrophobic cavity formed by domains I and II. The loop that connects the domains has another conserved amino acid motif, GPGCPVC. The cysteines in this motif form a disulfide bridge (SS1) in the crystal structure. HypD from *T. kodakaraensis* shows another disulfide bridge (SS2) in close proximity to SS1. However, the cysteines that form SS2 are not found in HypD from *E. coli* and are therefore not phylogenetically conserved.

HypC is structurally less complex than HypD. At 9.6 kDa, it consists of a flexible α-helix loop joined to a β-barrel. This

Received: March 8, 2013
Revised: April 18, 2013
Published: April 19, 2013

architecture is commonly referred to as an OB-fold.[17] HypC of *T. kodakaraensis* was crystallized and refined to 1.8 Å.[15] The N-terminus projects from the barrel and has a conserved cysteine "finger" at its end (C2). Another conserved residue is H51, which is in close spatial vicinity to C2, and they are located in a hydrophobic patch.

HypC and HypD form a tight complex, which was recently characterized structurally for the proteins from *T. kodakaraensis*.[14] The structure reveals that the β-barrel domain of HypC fits within the conserved hydrophobic niche of HypD. The residues C2 of HypC and C38 (C41 in *E. coli*) of the conserved CGxH motif in HypD are located at the HypCD interface and are within 5 Å of each other. Watanabe and co-workers presented a model in which a Fe ion is coordinated by C2 and C38, two CN^- ligands, and two unknown ligands and suggest that this might form the active site of HypD.[14] The anaerobically isolated HypCD complex from *E. coli*, which also contains sub-stoichiometric amounts of HypE, and from *Ralstonia eutropha* has revealed that the complex carries one CO and two CN^- ligands.[18,19] Moreover, the presence of the $(CN)_2CO$ group in the HypCD complex correlated strongly with two Fe ions additional to those associated with the [4Fe–4S] cluster of HypD,[19] suggesting that one of the Fe ions coordinated the CO and CN^- ligands.

It has been proposed previously that, while the function of HypC is to deliver the Fe-$(CN)_2CO$ cofactor to the apo-form of the hydrogenase large subunit, HypD is the scaffold on which the iron ion receives the CN^- ligands from HypE.[20,21] The HypD protein has also been proposed to be the enzyme that ultimately introduces the CO ligand. In this work, we present an FT-IR spectroscopic analysis of anaerobically purified HypD from *E. coli*. We demonstrate that purified HypD carries both CO and CN^- ligands and prove that these ligands are associated with a Fe ion. On the basis of site-directed mutagenesis coupled with FT-IR analyses, key amino acid residues shown previously for HypD to be essential for hydrogenase maturation[9,13] are suggested to form the active site of the complex. These findings are discussed in light of the recent crystal structure determinations of HypC, HypD, and the HypCD complex.

EXPERIMENTAL PROCEDURES

Bacterial Strains and Plasmids Used in This Study. The *E. coli* strains used during this study include MC4100,[22] DHP-D (Δ*hypD*), DHP-C (Δ*hypC*),[23] and BL21(DE3).[24] Plasmid pT-hypDEFCStrep[13] was used as source of the $HypC_{Strep}$–HypD complex. Furthermore, it was used as the template for site-directed mutagenesis using the Stratgene QuickChange procedure of the codons specifying C41, C69, C72, and E357 of HypD. The oligonucleotide primers used for site-directed mutagenesis are listed in Table S1 (Supporting Information).

Chromosomal DNA from MC4100 was used as the template for amplification of the *hypD* gene via PCR ($hypD_{fwd}$ 5′-CCCCATATGATGCGTTTTGTTGATGAATATCGC-3′ and $hypD_{rev}$ 5′-CCCAAGCTTTCACGCTTCACTCT-CCTGCTGAC-3′). The resulting DNA fragment was digested with NdeI and *Hin*dIII and ligated into pET28a, which was subsequently transformed into BL21(DE3) to overproduce $HypD_{His}$. Additionally, this plasmid was used as the template for site-directed mutagenesis of the codons specifying C41, C69, C72, and E357 of $HypD_{His}$.

Growth Conditions and Protein Overproduction. For overproduction of the $HypC_{Strep}$, $HypC_{Strep}D$, and $HypD_{His}$ protein variants, *E. coli* strain BL21(DE3) was transformed with plasmid phypC, pT-hypDEFCStrep, or phypD, respectively. Cells were grown in modified TB medium[19] containing 100 μg/mL of ampicillin or 50 μg/mL kanamycin, respectively, on a rotary shaker at 37 °C until an optical density of 0.4 at 600 nm was reached. Induction of gene expression was achieved by adding IPTG to a final concentration of 0.3 mM. After induction, the culture was incubated at 30 °C for a further 3–5 h. Cells were harvested after reaching an optical density at 600 nm of 1.0 by centrifugation for 30 min at 50 000*g* at 4 °C, and cell pellets were used either immediately or stored at −20 °C until use. For preparation of crude extracts to analyze in-gel hydrogenase enzyme activity, *E. coli* cells were cultivated anaerobically at 37 °C in buffered TYEP medium[25] supplemented with 0.8% (w/v) glucose as described previously.[26]

Preparation of Crude Extracts and Protein Purification. All steps were carried out under anaerobic conditions in an anaerobic chamber (Coy Laboratories, Grass Lake, USA) and at 4 °C unless stated otherwise. Wet cell paste from cells containing Strep-tagged HypC was resuspended at a ratio of 1 g per 3 mL of buffer W (100 mM Tris-HCl and 150 mM NaCl, pH 8.0) including 2 mM sodium dithionite, 5 μg DNase/mL, and 0.2 mM PMSF. Cells were disrupted by sonication (30 W for 5 min with 0.5 s pulses). Unbroken cells and debris were removed by centrifugation for 30 min at 50 000*g* at 4 °C, and the supernatant is henceforth referred to as the crude extract.

The crude extract derived from 10 g wet weight of cells was used for anaerobic purification of proteins. Proteins were isolated by chromatography on a StrepTactin-Sepharose column (8 mL; IBA, Göttingen, Germany) using gravity-flow. Unbound proteins were removed by washing the column with five column volumes of buffer W. Recombinant protein was eluted with buffer W including 5 mM desthiobiotin. Desthiobiotin was subsequently removed by passage through a series of Hi-Prep PD10 desalting columns (GE Healthcare) equilibrated with buffer W and connected to an ÄKTA apparatus (GE Healthcare). Proteins were eluted and concentrated by centrifugation at 7500*g* using centrifugal filters (Amicon Ultra, 50 K, Millipore, Eschborn, Germany).

His-tagged HypD protein variants were purified from BL21(DE3) transformed with the appropriate plasmid derivative. Wet cell paste was resuspended at a ratio of 1 g per 4 mL buffer A (50 mM Tris-HCl and 300 mM NaCl, pH 8.0). Crude extracts derived from approximately 5 g of wet cell paste were loaded onto a 1.5 × 10 cm column of Co^{2+}-charged resin (Talon resin, Clontech). The column, which had been previously equilibrated with buffer A was washed with five column volumes of the same buffer followed by three column volumes of buffer A supplemented with 10 mM imidazole and then three column volumes of buffer A supplemented with 20 mM imidazole to remove nonspecifically bound proteins. His-tagged proteins were subsequently eluted with buffer A containing 300 mM imidazole. Imidazole was removed by desalting as described above. His-HypD preparations were subjected to gel filtration chromatography step on a Superdex 200 gel filtration column (2.6 × 60 cm) equilibrated with buffer A.

Polyacrylamide Gel Electrophoresis and Protein Determination. Nondenaturing polyacrylamide gel electrophoresis (PAGE) using 7.5% (w/v) polyacrylamide with subsequent staining for hydrogenase enzyme activity was

performed as described.[27] SDS−PAGE was performed using 10 or 15% (w/v) polyacrylamide.[28]

FT-IR Spectroscopy. Fourier-transform infrared (FT-IR) spectroscopy was conducted on a Tensor27 (Bruker Optik, Ettlingen, Germany) equipped with a three-reflection silicon crystal attenuated total reflection (ATR) cell (Smith Detection, Warrington, USA) as described earlier.[19]

Oxidation of HypD by H_2O_2 was performed on wetted films. Samples were dried in a homemade acrylic glass cell on top of the ATR crystal plate to judge the amount of protein and integrity of the active site cofactors. Dry N_2 was passed through distilled water and was fed to the ATR gas cell in order to temper the protein film and make it available for further gas treatments. Another N_2 stream was passed through a saturated solution of H_2O_2 and passed across the semi-dry HypD film.

Nonheme Iron and Acid-Labile Sulfide Determination. Iron and acid-labile sulfide were determined as described previously.[29,30] Iron content was confirmed by inductively coupled plasma mass spectrometry (ICP-MS).[19] For ICP-MS analysis, 0.1 mg of purified protein (1 mg/mL) was used.

RESULTS

Overproduced and Purified HypD Has IR Signatures Characteristic of Metal-Bound CO and CN^- Ligands. HypD and variants with amino acid substitutions in key residues either were purified anaerobically as N-terminally His-tagged fusion proteins (see Experimental procedures) or were co-purified in complex with C-terminally Strep-tagged HypC, in which case HypD lacked a tag[13,19] (Figure 1). $HypC_{Strep}$ (Figure 1B) was purified as described previously.[13] Notably, His-HypD and its amino acid variants could be readily purified from anaerobic crude extracts of BL21(DE3) without contaminating HypC (Figure 1A), which was confirmed by Western blotting with anti-HypC antibodies (see Figure SI-1, Supporting Information). Moreover, His-HypD functionally complements a *hypD* mutation (see Figure 3 below).

Compared to HypCD, the infrared signature of HypD identified very similar bands in the range of 2200−1850 cm^{-1} (Figure 2a,b) but showed no contribution at 2337 cm^{-1} as previously observed for the HypCD complex.[19] Spectra were adjusted for amide II band height, and the bands corresponded well with published values[31,32] and can be assigned to CO (1956 cm^{-1}) and cyanide (CN^1 at 2072 cm^{-1} and CN^2 at 2092 cm^{-1}). HypC did not display any specific absorption in the range of 2200−1850 cm^{-1} (Figure 2c).

Identification of Amino Acid Residues in HypD That Are Important for CO and CN^- Binding. An extensive mutagenesis study of HypD carried out previously[20] identified cysteinyl residues C41, C69, and C72 as being essential for the maturation of active hydrogenases in *E. coli*. His-tagged HypD variants with C69A or C72A substitutions were purified (Figure 1A), and neither of these proteins revealed IR signatures in the 2200−1850 cm^{-1} range (Figure SI-2, Supporting Information). The same result was observed for the HypD variant in which C41 was exchanged for alanine, which was anticipated because the $HypCD^{C41A}$ complex also failed to exhibit any IR bands in the 2200−1850 cm^{-1} range.[19] The crystal structure of HypD revealed that glutamate 357 is located in the proximity of the putative active site.[14,15] Exchange of E357 to either alanine or aspartate in the variants $HypD^{E357A}$ and $HypD^{E357D}$ revealed an IR spectrum indistinguishable from that of native HypD (Figure SI-2, Supporting Information), indicating that E357 was dispensable for HypD function in hydrogen maturation.

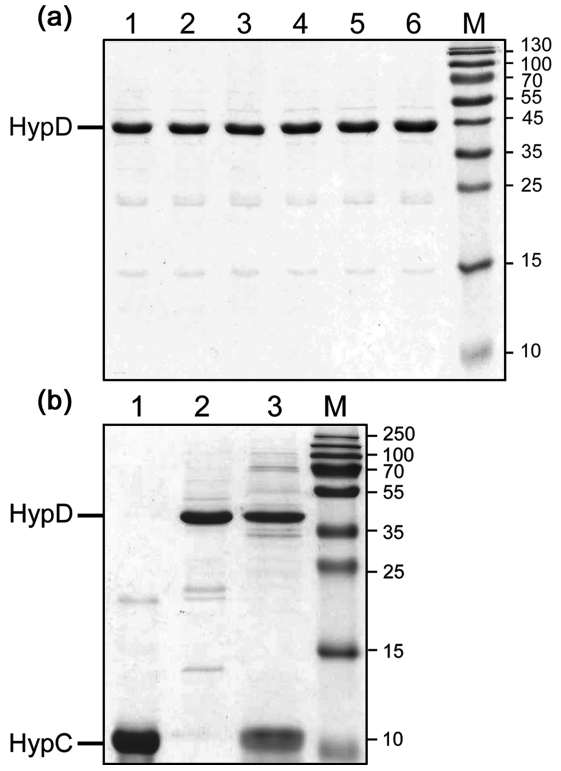

Figure 1. SDS analysis of proteins purified in this work. (a) Enriched HypD (5 μg of protein) after gel-filtration chromatography were separated by SDS−PAGE (15% w/v polyacrylamide) and stained with Coomassie Brilliant Blue. Lane 1, $HypD^{C72A}$; lane 2, $HypD^{C69A}$; lane 3, $HypD^{C41A}$; lane 4, $HypD^{E357D}$; lane 5, $HypD^{E357A}$; lane 6 $HypD^{wt}$; and lane M, PageRuler prestained molecular mass marker in kDa (Fermentas #SM0671/2). (b) Enriched HypC, HypD, and HypCD complex (5 μg of protein) were separated by SDS−PAGE (15% w/v polyacrylamide) and stained with Coomassie Brilliant Blue. Lane 1, $HypC_{Strep}$; lane 2, His-HypD; lane 3, $HypC_{Strep}$−HypD; lane M, PageRuler prestained marker in kDa (Fermentas #SM1811/2). The migration positions of HypD and HypC are indicated.

Infrared characterization of the HypD variants was supported by in-gel analysis of Hyd-1 and Hyd-2 hydrogenase activities in *E. coli* strains lacking *hypD* (DHP-D). Only variants that bound the $(CN)_2CO$ cofactor were able to restore hydrogenase activity in the respective strain, i.e., $HypD^{E357A}$ and $HypD^{E357D}$ in DHP-D, while the HypD variants with C41A, C69A, and C72A exchanges failed to restore enzyme activity (Figure 3).

Nonheme Iron Analysis Shows a Direct Correlation with the Presence of Bound $(CN)_2CO$ in HypD. The Fe and sulfide (S^{2-}) content of anaerobically purified native HypD and its variants was determined colorimetrically, and Fe was also analyzed by inductively coupled plasma mass spectrometry (ICP-MS). Native His-HypD typically showed five equivalents of Fe, with four sulfides per protein molecule (Table 1). Four of these iron ions are associated with the [4Fe−4S] cluster in HypD.[13,20] In a recent study, up to two additional Fe ions were found associated with the HypCD complex.[19] The additional Fe ion observed in His-HypD isolated in this study could therefore coordinate the $(CN)_2CO$ ligands, or it could be bound elsewhere in the protein. To demonstrate that the additional bound Fe ion was not due to nonspecific binding of iron to the protein, His-HypD was isolated without taking precautions to exclude oxygen and the nonheme Fe and sulfide content of the protein determined. Although the iron/sulfide

dx.doi.org/10.1021/bi400302v | *Biochemistry* 2013, 52, 3289−3296

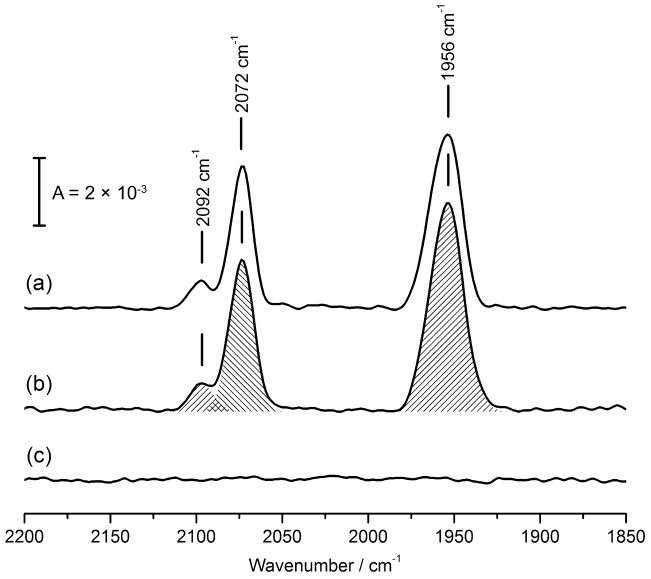

Figure 2. Infrared spectra of HypCD, HypD, and HypC. All samples were dried under N_2 and probed on a three-reflection silicon ATR crystal in the absence of O_2. The displayed spectra are the average of 4096 scans recorded at a spectral resolution of 4 cm^{-1}. Water absorption was subtracted by a broad spline function. (a) Spectrum of $HypCD^{wt}$. Bands fit to 1956 cm^{-1}, 2072 cm^{-1}, and 2092 cm^{-1}. These can be attributed to CO, CN^1, and CN^2, respectively. (b) Spectrum of $HypD^{wt}$. Bands fit to 1956, 2072, and 2092 cm^{-1} (hatching indicates the fit area). (c) Spectrum of $HypC^{wt}$. The sample does not show absorption in the region from 2200−1850 cm^{-1}.

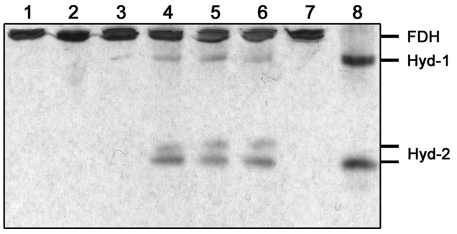

Figure 3. In-gel hydrogenase activity analysis of HypD amino acid variants. Crude extracts (50 μg of protein) derived from the strain DHP-D (Δ*hypD*) transformed with plasmids encoding HypD variants were analyzed for Hyd-1 and Hyd-2 enzyme activities after separation in native PAGE (7.5% w/v) under nondenaturing conditions followed by staining for hydrogenase activity. The stained bands corresponding to active Hyd-1 and Hyd-2 are indicated. Hydrogenase-independent activity due to hydrogen-oxidizing side reaction of formate dehydrogenase is indicated as FDH and acted as a loading control. Lane 1, DHP-D/pD^{C72A}; lane 2, DHP-D/pD^{C69A}; lane 3, DHP-D/pD^{C41A}; lane 4, DHPD/pD^{E357D}; lane 5, DHP-D/pD^{E357A}; lane 6, DHP-D/pD^{wt} lane 7, DHP-D (ΔhypD); and lane 8, 12 μg of extract derived from MC4100 (wt) were used.

ratio was one (Table 1), both determined values were below four, suggesting that the [4Fe−4S] site likely suffered oxidative damage. ICP-MS determination of Fe agreed with the result of chemical analysis. Note that HypD isolated aerobically showed no bands assignable to CO or CN^- (data not shown).

Substitution of amino acid cysteinyl residues 69, 72, or 41 individually with alanine reduced the Fe content from five to four (Table 1). In contrast, $HypD^{E357A}$ and $HypD^{E357D}$ showed an Fe content only slightly lower compared to that observed for the native protein. The Fe concentration was nevertheless clearly above 4 mol/mol HypD (determined both colorimetrically and by ICP-MS analysis). The sulfide content of the proteins was not markedly affected by substitution of the cysteinyl residues 69, 72, or 41 (Table 1). Taken together, these data indicate that all three cysteines are essential for stable association of the additional nonheme Fe ion with isolated HypD.

Table 1. Iron and Sulfide Concentration in HypD and Variants

	protein sample	nonheme Fe[a]	sulfide[a]
colorimetric	HypD	4.9 ± 0.45	4.1 ± 0.11
	HypD (aerob)	3.1 ± 0.3	3.1 ± 0.4
	$HypD^{C72A}$	3.8 ± 0.35	3.6 ± 0.27
	$HypD^{C69A}$	3.9 ± 0.22	3.8 ± 0.31
	$HypD^{C41A}$	4.04 ± 0.2	3.5 ± 0.27
	$HypD^{E357D}$	4.44 ± 0.8	3.62 ± 0.53
	$HypD^{E357A}$	4.53 ± 0.37	3.44 ± 0.42
ICP-MS	HypD	4.63 ± 0.24	n.d.
	HypD (aerob)	2.88 ± 0.15	n.d.
	$HypD^{C72A}$	3.66 ± 0.06	n.d.
	$HypD^{C69A}$	3.6 ± 0.16	n.d.
	$HypD^{C41A}$	3.7 ± 0.03	n.d.
	$HypD^{E357D}$	4.29 ± 0.16	n.d.
	$HypD^{E357A}$	4.44 ± 0.06	n.d.

[a]in [mol/mol protein]

Hydrogen Peroxide-Dependent Oxidation of HypD Provides Evidence That Fe Coordinates the CO and CN^- Ligands. To establish further the correlation between Fe coordination and CO and CN^- ligand binding, we performed an EDTA (ethylenediaminetetraacetic acid) titration with native His-HypD. EDTA releases ferrous iron from proteins with which it forms stable complexes.[33] HypD tolerated a 4-fold molar excess of EDTA after an incubation time of 5 min. For all higher concentrations of EDTA, the observed active site IR signatures were lost (data not shown).

His-HypD was rapidly oxidized by H_2O_2 (Figure 4). The FT-IR difference spectrum of $HypD_{red}$ versus $HypD_{ox}$ revealed negative bands, which, after fitting, could be assigned to CO (1956 cm^{-1}) and CN^1 (2072 cm^{-1}) for $HypD_{red}$. The spectrum also revealed a negative contribution at 1928 cm^{-1}, which can be assigned to CO. This band has not been seen previously in [NiFe]-hydrogenases, but contributions at similar energies were described for Fe(I)-CO in the reduced H-cluster of [FeFe]-hydrogenases.[34,35] Positive bands representing $HypD_{ox}$ included CO (1990 cm^{-1}), CN^1 (2092 cm^{-1}), and CN^2 (2112 cm^{-1}). When compared to $HypD_{red}$, this corresponds to a shift of +34 cm^{-1} for CO and +20 cm^{-1} for CN^1 and CN^2. It is important to note that the disappearance of CN^2 ($HypD_{red}$, see Figure 1b) was masked by an increase of CN^1 ($HypD_{ox}$) at the same band position. The oxidation was not reversible. See Figure SI-3 (Supporting Information) for an individual spectrum of $HypD_{ox}$.

To follow the oxidation kinetics more precisely, it was necessary to minimize the contact time of HypD with H_2O_2. To achieve this, a stream of dry N_2 was passed through a 30% solution of H_2O_2 in water. This aerosol was fed to a film of HypD. Figure 5 shows the redox-dependent decrease of the 1956 cm^{-1} (CO_{red}) and increase of the 1990 cm^{-1} (CO_{ox}) bands over time. Intensities are plotted relative to 1900 cm^{-1}. The respective kinetics are fitted exponentially with t = 29.72 for CO_{red} (R = 0.99, dotted line) and t = 27.82 for CO_{ox}. (R = 0.98, short dots). Furthermore, the kinetic data for the redox

dx.doi.org/10.1021/bi400302v | *Biochemistry* 2013, 52, 3289−3296

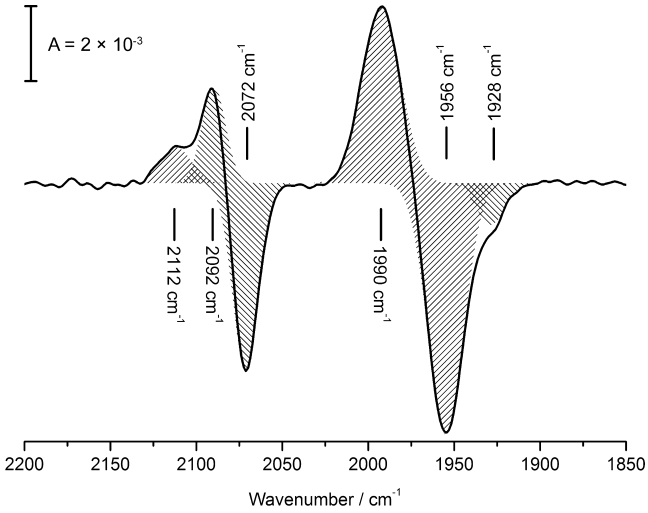

Figure 4. FT-IR difference spectrum of $HypD_{red}$ versus $HypD_{ox}$. A sample of HypD was dried under N_2 and probed on a three-reflection silicon ATR crystal in the absence of O_2. The spectrum was used as background with an average of 4096 scans recorded at a spectral resolution of 4 cm^{-1}. The film was treated with H_2O_2 aerosol (see Experimental Procedures) for 60 min and re-dried under N_2. The difference spectrum shows ligand contributions from $HypD_{red}$ (negative) and $HypD_{ox}$ (positive). Carbonmonoxide as bound to $HypD_{red}$ (1956 cm^{-1}) is lost in favor of CO_{ox} (1990 cm^{-1}). A small negative contribution at 1928 cm^{-1} can be attributed to a stronger reduced species of HypD. The band does not appear in $HypD_{ox}$. A peak at 2072 cm^{-1} (CN^1_{red}) shifts to 2092 cm^{-1} (CN^1_{ox}). The contribution at 2092 cm^{-1} appears decreased in comparison to 2072 cm^{-1} because it overlaps with the 2092 cm^{-1} band of CN^2_{red} which shifts to 2112 cm^{-1} in the difference spectrum. See Figure SI-2 (Supporting Information) for individual spectra of $HypD_{red}$ and $HypD_{ox}$.

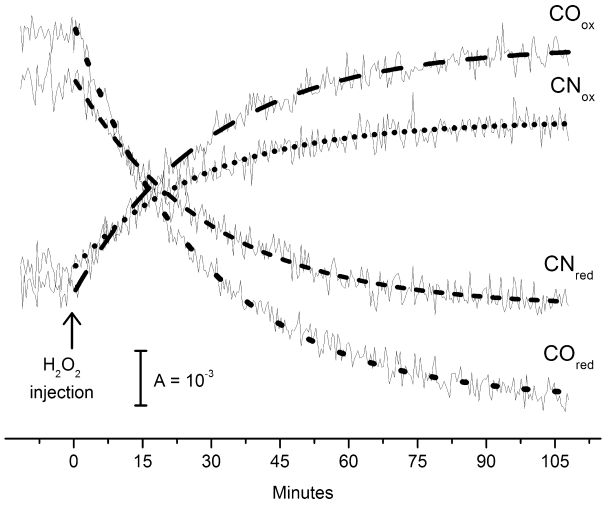

Figure 5. Kinetics of the individual peak height of CO and CN^1 during oxidation. A sample of HypD was dried under N_2 and probed on three-reflection silicon ATR crystal in the absence of O_2. Over the course of ~100 min, spectra with an average of 128 scans were recorded every ~24 s. At $t = 0$, the purging gas was sent through a 30% solution of H_2O_2 and the aerosol fed to the film (see Experimental Procedures). The decrease of band positions representing CO_{red} (1956 cm^{-1}) and CN^1_{red} (2072 cm^{-1}) is plotted against the increase of CO_{ox} (1990 cm^{-1}) and CN^1_{ox} (2092 cm^{-1}) over time. The respective kinetics are fitted exponentially with $t = 29.72$ for CO_{red} ($R = 0.99$, dotted line), $t = 27.82$ for CO_{ox}. ($R = 0.98$, short dots), $t = 29.1$ for CN^1_{red} ($R = 0.97$, dashed line), and $t = 28.2$ for CN^1_{ox}. ($R = 0.93$, short dashes).

transition of CN^1 (2072 cm^{-1}/ 2092 cm^{-1}) can be observed (Figure 5). Intensities are plotted relative to 2150 cm^{-1}. The respective kinetics were fitted exponentially with $t = 29.1$ for CN^1_{red} ($R = 0.97$, dashed line) and $t = 28.2$ for CN^1_{ox}. ($R = 0.93$, short dashes). From the direct comparison of the reaction kinetics, it is clear that CO and CN^- are subject to similar redox chemistries. The analysis hints at a shared ligand whose redox transition simultaneously affects CO and CN^-.

DISCUSSION

In this study, we demonstrate that HypD isolated from *E. coli* strain BL21(DE3) carries the complete Fe-$(CN)_2CO$ cofactor. The IR signatures perfectly resemble those of the spectrum observed for the recently isolated $HypC_{Strep}$–HypD complex.[18,19] While HypC is absolutely essential for the generation of $(CN)_2CO$ signals *in vivo*,[9,23] the findings of this work strongly suggest that HypD acts as the scaffold on which the Fe-$(CN)_2CO$ cofactor is formed. The CO (1956 cm^{-1}) and CN^1/ CN^2 (2072/2092 cm^{-1}) bands were detected with negligible variation between HypD and HypCD. As coulomb interactions of the HypC side chains with CO or CN^- would influence the vibration energy of ligands and shift their signature bands, the comparison of the spectra suggests that HypC is not required to stabilize the complex. Moreover, because current evidence suggests that one role of HypC is to deliver the completed Fe-$(CN)_2CO$ cofactor to its destination substrate, the apo-form of the HycE protein,[9,21] the findings of this study support this function. It is well documented that HypD can be isolated without associated HypC[13] and that purification of HypCD necessitates co-expression of the *hypC* and *hypD* genes,[36] which explains why we could isolate overproduced HypD in the absence of HypC. Nevertheless, HypC appears to have an important function in the formation of the Fe-$(CN)_2CO$ cofactor because it was noted that the amount of HypD isolated from BL21(DE3) cells was significantly lower when HypC was not co-overproduced with HypD. Approximately ten-fold less soluble HypD was isolated, while the bulk of the HypD was found in inclusion bodies. To date, it has not been possible to isolate HypC with bound CO or CN^- ligands, suggesting that the cofactor-bound form of the protein is highly unstable, perhaps requiring complex formation with both HypD and the apo-hydrogenase large subunit to effect its function in cofactor transfer.

The crystal structure of HypD from *Thermococcus kodakaraensis* revealed a [4Fe–4S] cluster in the C-terminal domain of the protein,[15] which confirmed the findings of earlier biochemical studies.[13,20] Moreover, the structure revealed two disulfide bridge motifs, referred to as SS1 (C69/72 based on the *E. coli* amino acid sequence) and SS2; however, the latter is not conserved in *Ec*HypD.[15] Apart from the [4Fe–4S] cluster, no additional cofactors were modeled into the electron density map, nor was any evidence for further cofactors obtained when the structures of the HypCD and HypCDE complexes from *T. kodakaraensis* were determined.[14] The isolation and crystallization of these protein complexes in the presence of air presumably resulted in loss of the highly oxygen-labile cofactors bound to the protein. The discovery of an IR signature reminiscent of the [NiFe]-hydrogenase active site on anaerobically prepared HydCD complex from both *E. coli*[18,19] and *Ralstonia eutropha*[18] suggested that both anaerobiosis and

dx.doi.org/10.1021/bi400302v | *Biochemistry* 2013, 52, 3289–3296

complex formation between HypC and HypD are necessary for cofactor integrity. The findings presented here confirm that anaerobiosis is essential for cofactor integrity but demonstrate that HypD is the principal carrier of the cofactor.

Cysteine 41 was reported previously to be essential for the appearance of the $(CN)_2CO$ signatures,[19] and our IR analysis of the $HypD^{C41A}$ supported this finding. Determination of Fe accounted for four equivalents on the $HypD^{C41A}$ variant rather than the five Fe ions identified for the native protein. Notably, however, HypD variants with amino acid substitutions of the highly conserved cysteines 69 and 72 also lacked the coordination of the CO and CN^- ligands, and both variants also revealed that four rather than five Fe ions were bound. These findings indicate that C69 and C72 are either necessary for cofactor coordination or play another role in cofactor biosynthesis, possibly coordinating the fifth Fe ion in isolated HypD. Analysis of hydrogenase enzyme activity confirmed that these variant enzymes could not restore hydrogenase activity to a *hypD* mutant. Notably, the HypCD complex revealed the presence of an additional sixth Fe ion, which could not be detected in the HypD analyzed here, suggesting that only the complex is able to stabilize binding of the sixth Fe ion. Studies are currently underway to determine whether HypC stabilizes Fe binding or whether it is involved in Fe delivery. Because cyanation of a tentative Fe ion in the HypCDE complex requires redox chemistry, it has been speculated[14,20] that the thiol groups of SS1 in the reduced state could serve as electron donors to the Fe. It is also conceivable that they coordinate the fifth Fe ion in the HypCD complex and that this is involved in electron transfer to the Fe atom coordinated by the CO and CN^- ligands. That a proximal glutamic acid identified in the structure of HypD[15] is required for redox catalysis by HypD could be ruled out by analysis of amino acid substitution of E357 to alanine or aspartate.

Direct demonstration that the CO and CN^- ligands are attached to Fe in HypD is somewhat complicated. Treatment of HypD with different concentrations of EDTA resulted in loss of the $(CN)_2CO$ signatures at a protein/EDTA ratio higher than four. Given that EDTA exclusively sequesters Fe, it can be concluded that the CO and CN^- ligands are associated with a Fe ion. Moreover, we were able to oxidize HypD with H_2O_2 and demonstrate an increase of 35 cm^{-1} and 20 cm^{-1} for the CO and CN^-, respectively. These shifts agree well with those predicted for Fe-bound ligands upon removal of an electron from the Fe.[37] During this Fenton reaction, H_2O_2 is reduced to $OH^\bullet$ and OH^-, while Fe(II) is oxidized to Fe(III).[38] Cyanide binds more strongly to Fe than CO and is affected less by changes of the redox state. Through determination of the virtual reaction constants of the oxidation reaction, it could be shown that both the increase of CO_{ox} and of CN^1_{ox} over CO_{red} and CN^1_{red} followed the same kinetic behavior, which is indicative of a concerted oxidation rather than individual reactions with CO and CN^-.

It is interesting to reconsider recent reaction models in light of these new findings. Watanabe and co-authors proposed a mechanism that includes coordination of Fe by C2 of HypC and C41 of HypD.[14] Two CN^- ligands are transferred to Fe by stepwise reduction of a specifically cyanated cysteinyl residue on HypE (the model accounts for a 2:1 ratio of HypE over HypCD). With CN^1, CN^2, and two cysteinyl ligands, the Fe ion is left with two unknown ligands "X" on HypCD (the authors suggest a low-spin Fe site in octahedral configuration). While CO probably occupies one of these unknown ligands, the final ligand is unknown. In this context, it is important to consider HypD residues that could potentially replace HypC-C2 in metal binding. Current evidence supports the role of C2 of HypC in coordinating the Fe-$(CN)_2CO$ cofactor, and this has been discussed at length.[9,14,36] In the vicinity of C41, the strongly conserved histidines H44 and H201 (*E. coli* numbering) might serve this role, although HypD mutants with individual substitution in these residues retained maturation activity.[20] The effects of exchanging H44 and/or H201 on the IR signatures have yet to be examined. Cysteine 41 and H44 are part of the CGxH motif, while H201 can be found in the PxHVS motif.[15] With residues C2 and H51 (HypC) and C41 and H44/H201 (HypD), a tetrahedral Fe complex can be formed, reminiscent of the high-spin Fe sites on rubredoxin and superoxide reductase.[39] The role of H51 is ambiguous, however, as amino acid exchange of this residue to different amino acids resulted in variable phenotypes *in vivo*.[40] Hence, Figure 6 depicts an unknown ligand as the second

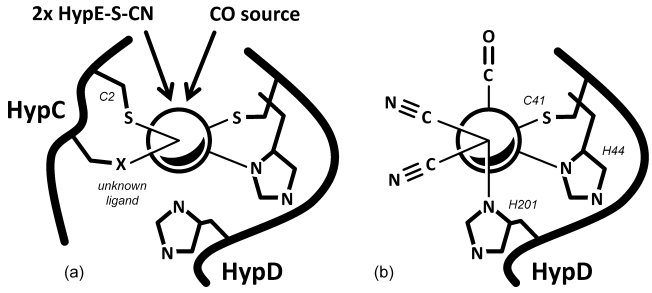

Figure 6. Cartoon model of Fe ligation in a transient HypCD complex and mature HypD. We propose that HypC and HypD collectively bind a single Fe ion through conserved cysteine and histidine residues. Iron is likely to adopt a tetrahedral geometry in such a ligation environment.[39] For HypC, the role of H51 was discussed, but its role remains ambiguous; thus, the model includes an unknown ligand (Figure 6a; see text for details). The transfer of CN^- or CO switches the Fe site from high- to low-spin and triggers a change in coordination geometry. Successive addition of CN^- and CO replaces HypC as the ligation partner in the mature complex (Figure 6b). Cyanide is delivered by HypE, while the source of carbon monoxide remains to be determined.

coordination partner to Fe on HypC. Although they appear not to be within ligation distance in the crystal structure of HypCD, C69/C72 might play a role in metal binding. It can be expected that the active site fold of HypCD adopts a different arrangement with Fe-$(CN)_2CO$ bound. Additionally, the role of C69/C72 (S1) in redox chemistry[14] needs to be addressed as this motif can only deliver two electrons to a process that ultimately demands four reducing equivalents. It is conceivable that the [4Fe−4Fe] cluster could play a key role in this context.

When HypE enters the complex and transfers its cyanide group to the Fe site on HypCD,[11] the complex must become low-spin and adopt octahedral geometry. Upon transfer of a second CN^- group and the CO ligand to Fe, the metal ion cannot maintain its original amino acid ligation. By demonstrating that HypD can coordinate the Fe-$(CN)_2CO$ cofactor without HypC, we raise the question as to the geometry of the cofactor in HypD. Cysteine 41 occupies the fourth ligand as our experiments confirm, and although no definite conclusion can be drawn regarding the identity of the remaining two ligands, C69 and C72 could be shown here to be essential to maturation activity. Structurally, H44 and H201

also present themselves as candidates for the fourth and fifth ligands. Figure 6a shows a cartoon model of the transient HypCD complex that carries an active high-spin Fe ion. Transfer of CN^- triggers the iron site to change its coordination geometry, and the ligands provided by HypC are successively replaced by cyanide and carbon monoxide ligands (Figure 6b), leaving the Fe-$(CN)_2CO$ cofactor assembly on the scaffold HypD.

Using FT-IR spectroscopy, we could show that HypD can bind the Fe-$(CN)_2CO$ cofactor stably without the assistance of HypC. Although HypC appears to support the generation of the Fe-$(CN)_2CO$ cofactor, HypC itself could not be isolated with bound CO or CN^- ligands. The identification of the Fe-$(CN)_2CO$ cofactor associated with HypD contrasts the findings of the structural analysis of HypD, HypCD, and HypCDE complexes, none of which shows electron density for a Fe-$(CN)_2CO$ cofactor. However, this is probably due to the labile nature of cofactor binding.

We provide spectroscopic evidence for the essential nature of cysteinyl residues 69 and 72 in both Fe and $(CN)_2CO$ binding. Taken together, all of these data support the notion that HypD is directly involved in the catalytic generation of $(CN)_2CO$.

External Fe is not found in the HypD crystal structures, but key residues of HypD form a cavity near the HypC−HypD interface, which is likely to provide coordination to a low-spin octahedral Fe ion. Our study demonstrates for the first time the actual presence of Fe on HypD in addition to the Fe in the [4Fe−4S] cluster. Cysteines 41, 69, and 72 of HypD are all required for binding of the Fe-$(CN)_2CO$ cofactor.[18,19] The transfer of a strong-field ligand like CN^- to Fe on HypCD can trigger a change of the coordination complex and liberate HypC from HypD. The origins of the Fe in the cofactor and the CO ligand remain to be elucidated.

■ ASSOCIATED CONTENT

Supporting Information

List of oligonucleotide primers used in the generation of HypD variants; SDS−PAGE and Western blot analysis; infrared spectra of HypD variants; and infrared spectrum of $HypD_{ox}$. This material is available free of charge via the Internet at http://pubs.acs.org.

■ AUTHOR INFORMATION

Corresponding Author

*Phone: +49 30 838 55069. E-mail: svenstripp@zedat.fu−berlin.de.

Funding

This study was supported by EFRE funds of the EU and the DFG (Grant SA 494/3-1, 3-2) to R.G.S. and by the BMBF (H_2 design cells) to J.H.

Notes

The authors declare no competing financial interest.

■ ACKNOWLEDGMENTS

We gratefully acknowledge August Böck for providing the antiserum against *E. coli* HypC and Constanze Pinske for discussions.

■ REFERENCES

(1) Vignais, P. M., and Billoud, B. (2007) Occurrence, classification, and biological function of hydrogenases: an overview. *Chem. Rev. 107*, 4206−4272.

(2) Thauer, R. K., Kaster, A.−K., Goenrich, M., Schick, M., Hiromoto, T., and Shima, S. (2010) Hydrogenases from methanogenic archaea, nickel, a novel cofactor, and H2 storage. *Annu. Rev. Biochem. 79*, 507−536.

(3) Volbeda, A., Charon, M. H., Piras, C., Hatchikian, E. C., Frey, M., and Fontecilla−Camps, J. C. (1995) Crystal structure of the nickel−iron hydrogenase from *Desulfovibrio gigas*. *Nature 373*, 580−587.

(4) Nakamoto, K., and Czernuszewicz, R. S. (1993) Infrared Spectroscopy, in *Methods in Enzymology* (Riordan, J. F., and Vallee, B. L., Eds.) pp 259−289, Academic Press, San Diego, CA.

(5) Bagley, K., Van Garderen, C., Chen, M., Duin, E., Albracht, S., and Woodruff, W. (1994) Infrared studies on the interaction of carbon monoxide with divalent nickel in hydrogenase from *Chromatium vinosum*. *Biochemistry 33*, 9229−9236.

(6) Bagley, K., Duin, E., and Roseboom, W. (1995) Infrared−detectable group senses changes in charge density on the nickel center in hydrogenase from *Chromatium vinosum*. *Biochemistry 34*, 5527−5535.

(7) Van der Spek, T. M., Arendsen, A. F., Happe, R. P., Yun, S., Bagley, K. A., Stufkens, D. J., Hagen, W. R., and Albracht, S. P. (1996) Similarities in the architecture of the active sites of Ni−hydrogenases and Fe−hydrogenases detected by means of infrared spectroscopy. *Eur. J. Biochem. 237*, 629−34.

(8) Happe, R., Roseboom, W., and Plerik, A. (1997) Biological activation of hydrogen. *Nature 385*, 126.

(9) Böck, A., King, P. W., Blokesch, M., and Posewitz, M. C. (2006) Maturation of Hydrogenases, in *Advances in Microbial Physiology* (Poole, R. K., Ed.) Vol. *51*, pp 1−71, Academic Press, San Diego, CA.

(10) Olson, J. W., Mehta, N. S., and Maier, R. J. (2001) Requirement of nickel metabolism proteins HypA and HypB for full activity of both hydrogenase and urease in *Helicobacter pylori*. *Mol. Microbiol. 39*, 176−182.

(11) Reissmann, S., Hochleitner, E., Wang, H., Paschos, A., Lottspeich, F., Glass, R. S., and Böck, A. (2003) Taming of a poison: biosynthesis of the NiFe−hydrogenase cyanide ligands. *Science 299*, 1067−1070.

(12) Paschos, A., Bauer, A., Zimmermann, A., Zehelein, E., and Böck, A. (2002) HypF, a carbamoyl phosphate−converting enzyme involved in [NiFe] hydrogenase maturation. *J. Biol. Chem. 277*, 49945−49951.

(13) Blokesch, M., Albracht, S. P. J., Matzanke, B. F., Drapal, N. M., Jacobi, A., and Böck, A. (2004) The complex between hydrogenase−maturation proteins HypC and HypD is an intermediate in the supply of cyanide to the active site iron of [NiFe]−hydrogenases. *J. Mol. Biol. 344*, 155−167.

(14) Watanabe, S., Matsumi, R., Atomi, H., Imanaka, T., and Miki, K. (2012) Crystal structures of the HypCD complex and the HypCDE ternary complex: transient intermediate complexes during [NiFe] hydrogenase maturation. *Structure 20*, 2124−2137.

(15) Watanabe, S., Matsumi, R., Arai, T., Atomi, H., Imanaka, T., and Miki, K. (2007) Crystal structures of [NiFe] hydrogenase maturation proteins HypC, HypD, and HypE: insights into cyanation reaction by thiol redox signaling. *Mol. Cell 27*, 29−40.

(16) Rossmann, M. G., Moras, D., and Olsen, K. W. (1974) Chemical and biological evolution of a nucleotide-binding protein. *Nature 250*, 194−199.

(17) Murzin, A. G. (1993) OB (Oligonucleotide/ oligosaccharide binding)-fold: common structural and functional solution for non−homologous sequences. *EMBO J. 12*, 861−867.

(18) Bürstel, I., Siebert, E., Winter, G., Hummel, P., Zebger, I., Friedrich, B., and Lenz, O. (2012) A universal scaffold for synthesis of the Fe(CN)2(CO) moiety of [NiFe]−hydrogenase. *J. Biol. Chem. 2*, 1−19.

(19) Soboh, B., Stripp, S. T., Muhr, E., Granich, C., Braussemann, M., Herzberg, M., Heberle, J., and Sawers, R. G. (2012) [NiFe]−hydrogenase maturation: isolation of a HypC−HypD complex carrying diatomic CO and CN−ligands. *FEBS Lett. 586*, 3882−3887.

(20) Blokesch, M., and Böck, A. (2006) Properties of the [NiFe]−hydrogenase maturation protein HypD. *FEBS Lett. 580*, 4065−4068.

(21) Forzi, L., and Sawers, R. G. (2007) Maturation of [NiFe]–hydrogenases in *Escherichia coli*. *BioMetals 20*, 565–578.
(22) Casadaban, M. J. (1976) Regulation of the regulatory gene for the arabinose pathway, araC. *J. Mol. Biol. 104*, 557–566.
(23) Jacobi, A., Rossmann, R., and Böck, A. (1992) The hyp operon gene products are required for the maturation of catalytically active hydrogenase isoenzymes in *Escherichia coli*. *Arch. Microbiol. 58*, 444–451.
(24) Studier, F. W., and Moffatt, B. A. (1986) Use of bacteriophage T7 RNA polymerase to direct selective high–level expression of cloned genes. *J. Mol. Biol. 189*, 113–130.
(25) Begg, Y. A., Whyte, J. N., and Haddock, B. A. (1977) The identification of mutants of *Escherichia coli* deficient in formate dehydrogenase and nitrate reductase activities using dye indicator plates. *FEMS Microbiol. Lett. 2*, 47–50.
(26) Pinske, C., and Sawers, R. G. (2012) A–type carrier protein ErpA is essential for formation of an active formate–nitrate respiratory pathway in *Escherichia coli* K–12. *J. Bacteriol. 194*, 346–353.
(27) Ballantine, S. P., and Boxer, D. H. (1985) Nickel–containing hydrogenase isoenzymes from anaerobically grown *Escherichia coli* K–12. *J. Bacteriol. 163*, 454–459.
(28) Laemmli, U. K. (1970) Cleavage of structural proteins during the assembly of the head of bacteriophage T4. *Nature 227*, 680–685.
(29) Cline, J. D. (1969) Spectrophotometric determination of hydrogen sulfide in natural waters. *Limnol. Oceanogr. 14*, 454–458.
(30) Fish, W. W. (1988) Rapid Colorimetric Micromethod for the Quantitation of Complexed Iron in Biological Samples, in *Methods in Enzymology* (Riordan, J. F., and Vallee, B. L., Eds.) pp 357–364, Academic Press, San Diego, CA.
(31) Pierik, A. J., Roseboom, W., Happe, R. P., Bagley, K. A., and Albracht, S. P. J. (1999) Carbon monoxide and cyanide as intrinsic ligands to iron in the active site of [NiFe]–hydrogenases. *J. Biol. Chem. 274*, 3331–3337.
(32) De Lacey, A. L., Pardo, A., Fernández, V. M., Dementin, S., Adryanczyk-Perrier, G., Hatchikian, E., and Rousset, M. (2004) FTIR spectroelectrochemical study of the activation and inactivation processes of [NiFe] hydrogenases: effects of solvent isotope replacement and site-directed mutagenesis. *J. Biol. Chem. 9*, 636–642.
(33) Auld, D. S. (1995) Removal and Replacement of Metal Ions in Metallopeptidases, in *Methods in Enzymology* (Barett, A. J., Ed.) pp 228–242. Academic Press, San Diego, CA.
(34) Silakov, A., Kamp, C., Reijerse, E., Happe, T., and Lubitz, W. (2009) Spectroelectrochemical characterization of the active site of the [FeFe] hydrogenase HydA1 from *Chlamydomonas reinhardtii*. *Biochemistry 48*, 7780–6.
(35) Roseboom, W., De Lacey, A. L., Fernandez, V. M., Hatchikian, E. C., and Albracht, S. P. J. (2006) The active site of the [FeFe]–hydrogenase from Desulfovibrio desulfuricans. II. Redox properties, light sensitivity and CO–ligand exchange as observed by infrared spectroscopy. *J. Biol. Inorg. Chem. Soc. 11*, 102–18.
(36) Blokesch, M., and Böck, A. (2002) Maturation of [NiFe]–hydrogenases in *Escherichia coli*: the HypC cycle. *J. Mol. Biol. 324*, 287–296.
(37) Volbeda, A., and Fontecilla-Camps, J. (2003) The active site and catalytic mechanism of NiFe hydrogenases. *Dalton Trans. 21*, 4030–4038.
(38) Wink, D. A., Nims, R. W., Saavedra, J. E., Utermahlen, W. E., and Ford, P. C. (1994) The Fenton oxidation mechanism: reactivities of biologically relevant substrates with two oxidizing intermediates differ from those predicted for the hydroxyl radical. *Proc. Natl. Acad. Sci. U.S.A. 91*, 6604–6608.
(39) Kurtz, D. M. (2006) Avoiding high–valent iron intermediates: superoxide reductase and rubrerythrin. *J. Inorg. Biochem. 100*, 679–693.
(40) Blokesch, M. (2004) *[NiFe]-Hydrogenasen von Escherichia coli: Funktionen der am Metalleinbau beteiligten Proteine*, Ludwig-Maximilians-Universität München, München, Germany.